Available online at www.sciencedirect.com
ScienceDirect
Thermochimica Acta 460 (2007) 77–84
thermochimica acta
www.elsevier.com/locate/tca

Model-free kinetics analysis of decomposition of polypropylene over Al-MCM-41

B. Saha, A.K. Ghoshal *

Department of Chemical Engineering, Indian Institute of Technology Guwahati, Guwahati 39, Assam, India

Received 29 January 2007; received in revised form 8 May 2007; accepted 21 May 2007
Available online 24 May 2007

Abstract

Both thermal and catalytic decomposition of PP sample is studied to understand the effect of catalyst (Al-MCM-41) on the decomposition behaviour. Mesoporous catalyst (Al-MCM-41) is synthesized by sol–gel methods and characterized by X-ray diffraction (XRD) analysis and nitrogen adsorption study. The optimum catalyst composition is found to be around 18.5 wt%, where the reduction in maximum decomposition temperature is around 103 °C. The nonlinear Vyazovkin model-free technique is applied to evaluate the quantitative information on variation of E_α with α for PP sample under both catalytic and noncatalytic nonisothermal conditions.

The constant pattern behaviour of the TG curves and the similar trend on variation of E_α with α for both catalytic and noncatalytic decomposition of PP indicates similar mechanism involved during decomposition. The only effect of catalyst is observed in the form of reduction of the temperature and the activation energy. The literature reported data on such variation are compared with the results of the present study. Results show that Al-MCM-41 is superior to the ZSM-5 catalyst in terms of catalyst loading due to the existence of larger external macropore and mesopore surface in it.

Keywords: Activation energy; Al-MCM-41; Catalytic decomposition; Model-free analysis; Polypropylene

1. Introduction

Catalytic pyrolysis of waste plastics is a subject of growing interest on the perspective of solid waste management since they are an alternative source of energy or chemical raw materials. Zeolite based catalysts reduce decomposition temperature, decrease activation energy, and produce more gaseous/lighter products including the light olefins and aromatic fractions. But mesoporous catalysts accelerate the degradation process with production of low proportion of aromatics and a higher content of olefin and paraffin species. Several authors reported promising results on the catalytic pyrolysis of polypropylene over catalysts, such as ZSM-5 [1–5], ZSM-12 [3], DeLaZSM-5 [4], BEA [5], MOR [5], HZSM-5 [6–9], PZSM-5 [6,9], HMOR [8], HUSY [8], US-Y [1,4,10], Beta [11], FCC [1,10], pillared clay [1], and two mesoporous catalysts SAHA [8] and MCM-41 [7–8,12]. According to Marcilla et al. [7], mesoporous catalysts (MCM-41b) with a greater pore size and higher acidity with high aluminium content was the most active one for the pyrolysis of PP. Highly olefinic product with a wide carbon number distribution during MCM-41 and SAHA catalyzed pyrolysis of PP were found by Lin and Yen [8].

Recently, mesoporous catalysts (Al-MCM-41) synthesized either by sol–gel or by hydrothermal method have been used for decomposition of HDPE and LDPE to analyze the decomposition products [13–15]. However, much less articles are referred to the effect of MCM-41 on PP [7].

The pyrolysis kinetics study is important to know the decomposition mechanism, rate of reaction, reaction parameters and to predict the products distribution. This in turn helps in proper selection of reactor, optimization of the reactor design and operating conditions. Model-free analysis technique is advantageous over model-fitting analysis when the real kinetics mechanism is unknown. This becomes extremely important during catalytic decomposition since reaction mechanism may change drastically with type and concentration of catalyst. Recently, Vyazovkin model-free kinetics technique has extensively been applied for many complex reaction processes to obtain reliable

* Corresponding author. Tel.: +91 361 2582251; fax: +91 361 2582291.
E-mail address: aloke@iitg.ernet.in (A.K. Ghoshal).

0040-6031/$ – see front matter © 2007 Elsevier B.V. All rights reserved.
doi:10.1016/j.tca.2007.05.016

and consistent kinetic information about the overall process [3,16–27]. Apart from this, isoconversion method presents a compromise between the single-step Arrhenius kinetic treatments and the prevalent occurrence of processes whose kinetics are multi-step or non-Arrhenius [25,26]. Thermal and catalytic decomposition kinetics studies of PP over BEA [5], ZSM-5 [3,5], MOR [5] and ZSM-12 [3] catalysts applying Vyazovkin model-free approach [3] and Kissinger approximation [5] based on multi-heating rates are reported in the literature.

In the present investigation, we studied both thermal and catalytic decomposition of PP sample. We have synthesized sol–gel Al-MCM-41 catalyst, characterized it and examined the optimum catalyst concentration (18.5 wt%) for decomposition of PP, after which reduction in maximum decomposition is relatively less. We applied the nonlinear Vyazovkin model-free technique to study the nonisothermal catalytic and noncatalytic decomposition of PP sample. We have also shown, probably the first time, the quantitative information on variation of E_α with α for PP sample under both catalytic (sol–gel Al-MCM-41) and noncatalytic nonisothermal conditions. The literature reported data on such variation under noncatalytic condition are compared with the present result.

2. Experimental

2.1. Synthesis of sol–gel Al-MCM-41 [28,29]

Sol–gel Al-MCM-41 catalyst was prepared according to the room temperature method described in literature [28,29] but with template, *N*-cetyle-*N*, *N*, *N* trimethylammonium bromide ($C_{19}H_{42}BrN$) in place of tetradecyltrimethylammonium bromide or hexadecyltrimethylammonium bromide. The chemicals used were $C_{19}H_{42}BrN$ (98%, Loba Chemie, India), tetraethoxysilane (TEOS (98%), Merck, Germany); aluminium isopropoxide (AIP (>98%), Acros Organics, India), 25% ammonia solution ((99.5%), Merck, India), propan-2-ol (PrOH) ((99.5%), Merck, India) and deionzied water. The template (1.29 g) was mixed with 69.2 g of water, warmed till complete dissolution, and allowed to cool down before adding 5 mL of ammonia. A mixture of 5 mL of TEOS with an appropriate volume of the AIP solution was added to this dropwise while stirring over a period of 15 min to achieve the required molar ratio. The molar composition of the gel was 1TEOS:1/*x*AIP:0.147C19TMABr:3.04NH_3:160H_2O:*y*PrOH, with $y = 2.89$ and $x = 30$. The suspension was kept under stirring for 1–1.2 h. The synthesized products were recovered by filtration and washed with about 2 L of deionized water. After drying at 343 K, the samples were calcined at 823 K for 8–12 hour at the heating rate of 2 K min^{-1}.

2.2. Characterization of Al-MCM-41 catalyst

The sol–gel Al-MCM-41 catalyst thus synthesized was characterized by X-ray diffraction (XRD) analysis and nitrogen adsorption study at 77 K. The XRD was carried out on Bruker AXS instrument using Cu Kα radiation (40 kV, 40 mA). Nitrogen adsorption isotherm at 77 K was determined on SA 3100 surface area analyzer from Beckman-Coulter using helium (for dead space calibration) and nitrogen. The Al-MCM-41 samples were out gassed for 3 h at 300 °C under nitrogen flow.

2.3. Catalytic and noncatalytic decomposition of PP over Al-MCM-41 catalyst (sol–gel)

The nonisothermal decomposition experiments with and without catalyst were carried out for polypropylene (PP) (polypropylene homopolymer (PPHP), Trade name: Koylene ADL, Grade AS030N) supplied by Indian Petrochemicals Corporation Limited, Vadodara, India with melt flow index 3.0. Experiments were carried out in a TGA instrument of Mettler TOLEDO with model no. TGA/SDTA 851^e under nitrogen atmosphere for a range of temperature 303–875 K. Nitrogen flow rate was maintained at 40–50 ml min^{-1} according to the specification of the equipment. PP samples were shredded into very small pieces and directly fed to the TGA instrument. Platinum crucible (150 μl) was used as sample holder. PP decomposition experiments were carried out with different percentage of catalysts (0–33 wt%) at 10 K min^{-1}. The optimum catalyst percentage was found around 18.5 wt% after which reduction in maximum decomposition temperature with increase in catalyst percentage was not so significant. Therefore, further catalytic decomposition experiments were carried out using 18.5 wt% catalysts (sol–gel Al-MCM-41) at different heating rates of 5, 10, 15, 20, and 25 K min^{-1}. The TGA experiments were repeated thrice at 10 °C heating rate without catalysts. The deviations observed are very little. However, the deviations are reported in terms of average relative deviation, $\mathrm{ARD}(\%) = (100/N)\sum_{i=1}^{N}|(x_i^{\mathrm{exp}} - x_{\mathrm{av},i})/x_{\mathrm{av},i}|$, where x_i^{exp} and $x_{\mathrm{av},i}$ are the experimental values of the variables (temperature and normalized mass) and average values of the variables, respectively. N is total number of data points for each experiment. Results show that ARD% is 0.005–0.019 (for temperature) and 0.041–0.1579 (for mass). Thermal decomposition (noncatalytic) experiments for PP were also conducted in dynamic condition at different heating rates of 5, 10, 15, 20 and 25 K min^{-1}.

3. Kinetics analysis

3.1. Model-free kinetics analysis

The kinetics model equation combined with the Arrhenius approach of the temperature function of reaction rate constant is expressed as:

$$\frac{\mathrm{d}\alpha}{\mathrm{d}t} = k_0 \exp\left(\frac{-E_\alpha}{RT}\right) f(\alpha) \quad (1)$$

where t is time (min), T the temperature (K), α the conversion of reaction $(W_0 - W)/(W_0 - W_\infty)$, W_0 the initial weight of the sample (mg), W the sample weight (mg) at any temperature T, W_∞ the final sample weight (mg), $\mathrm{d}\alpha/\mathrm{d}t$ the rate of reaction (min^{-1}), and $f(\alpha)$ is the reaction model. k_0, the pre-exponential factor (K^{-1}) and E_α, the activation energy (kJ mol^{-1}) are the Arrhenius parameters. R is the gas constant (kJ mol^{-1} K^{-1}). The reaction model may take various forms based on nucleation and

nucleus growth, phase boundary reaction, diffusion, and chemical reaction [19–22]. However, the present investigation does not require any information of reaction model since we report here decomposition kinetics using model-free approach.

At a constant heating rate under nonisothermal conditions the explicit temporal/time dependence in Eq. (1) is eliminated through the trivial transformation

$$\beta\frac{d\alpha}{dT} = k_0 \exp\left(\frac{-E_a}{RT}\right) f(\alpha) \quad (2)$$

where $\beta = dT/dt$ is the heating rate ($K\,min^{-1}$) and $d\alpha/dT$ is the rate of reaction (K^{-1}).

Rearrangement and integration of Eq. (2) leads to Eq. (3) as follows.

$$g(\alpha) = \frac{k_0}{\beta}\int_0^{T_\alpha} \exp\left(\frac{-E}{RT}\right) dT = \frac{k_0}{\beta} I(E, T_\alpha) \quad (3)$$

where $g(\alpha) = \int_0^\alpha [f(\alpha)]^{-1}\, d\alpha$.

Because $g(\alpha)$ is independent of heating rate, Eq. (3) can be written for a given conversion and a set of n experiments carried out at different heating rates β_i ($i = 1, \ldots, n$) as Eq. (4)

$$\frac{k_0}{\beta_1} I(E_\alpha, T_{\alpha,1}) = \frac{k_0}{\beta_2} I(E_\alpha, T_{\alpha,2}) = \cdots = \frac{k_0}{\beta_n} I(E_\alpha, T_{\alpha,n}) \quad (4)$$

Thus,

$$\sum_{i=1}^{n}\sum_{i\neq j}^{n} \frac{I(E_\alpha, T_{\alpha,i})\beta_j}{I(E_\alpha, T_{\alpha,j})\beta_i} = \text{constant} \quad (5)$$

Since the T_α values are measured with some experimental error, Eq. (4) can only be satisfied as an approximate equality. Therefore, the activation energy (E_α) can be determined at any particular value of α by finding the value of E_α for which the objective function $\Omega(E_\alpha)$ is minimized [24,25], where

$$\Omega(E_\alpha) = \sum_{i=1}^{n}\sum_{j\neq i}^{n} \frac{I(E_\alpha, T_{\alpha,i})\beta_j}{I(E_\alpha, T_{\alpha,j})\beta_i} \quad (6)$$

3.2. Model-free isoconversion method for nonisothermal experiments [3,16–27]

For a set of five experiments carried out at five different heating rates (5, 10, 15, 20 and 25 $K\,min^{-1}$), E_α is determined at any particular value of α by minimizing the objective function, Ω (Eq. (6)).

The temperature integral, $I(E_\alpha, T_{\alpha i}) = \int_0^{T_{\alpha i}} \exp(-E_\alpha/RT)\, dT$ is evaluated by direct numerical integration where the temperature integral takes the form

$$I(E_\alpha, T_{\alpha i}) = \int_0^{T_{\alpha i}} \exp\left(\frac{-E_\alpha}{RT}\right) dT = \frac{E_\alpha}{R}\left[\frac{\exp(-u)}{u} - Ei(u)\right] \quad (7)$$

where E_α/RT and $Ei(u) = \int_u^\infty ((\exp(-u))/u)\, du$.

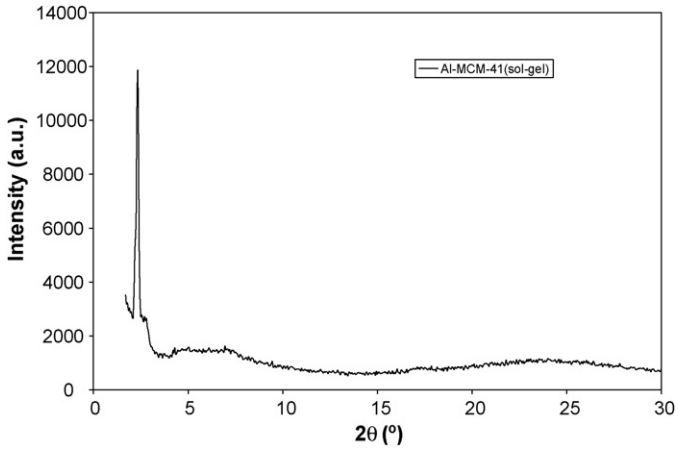

Fig. 1. XRD pattern of Al-MCM-41(sol–gel) catalyst (using step size = 0.05° and step time 0.5 s).

Details of development of Eq. (7), numerical procedure and algorithms for model-free technique are discussed in our recent publication [26].

4. Results and discussion

4.1. Characterization of Al-MCM-41 catalyst

The XRD spectra (Fig. 1) of calcined Al-MCM-41 (sol–gel) exhibit the low angle and intense diffraction peak between $2\theta = 2.1$–2.40° indicating the reflection of 1 0 0 plane [16]. No peak at higher angle was observed indicating the absence of any crystalline phase containing aluminium [29].

Nitrogen adsorption isotherm at 77 K of the catalyst is shown in Fig. 2. The catalyst presents a type IV isotherm according to IUPAC classification, typical of good quality mesoporous materials [16,29]. The desorption points, shown in the figure, exhibit a pore filling step within a fairly narrow range of P/P^0, indicating size uniformity of the tubular unidirectional mesopores [29]. Table 1 summarizes the textural properties of Al-MCM-41 catalyst prepared by sol–gel method. The pore size distribu-

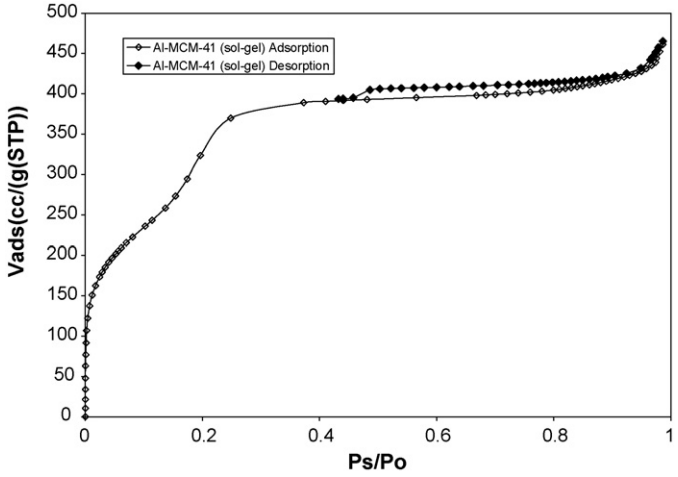

Fig. 2. Nitrogen adsorption isotherm at 77 K of Al-MCM-41 catalyst.

Table 1
Textural properties of Al-MCM-41 (sol–gel)

Properties	Values
BET surface area ($m^2\ g^{-1}$)	1202
Pore volume (at $P_s/P_o = 0.9814$ (adsorption) ($cm^3\ g^{-1}$)	0.7005
Micropore volume (by *t*-plot surface area) ($cm^3\ g^{-1}$)	0.0
Si/Al ratio	35.6

tion was calculated using the Barrett–Joyner–Halenda (BJH) model applied to the adsorption branch of the isotherm, assuming cylindrical pore geometry. It was found that the pore sizes lie within 4 nm (Fig. 3). The total distribution is not available due to limitation of the instrument to measure pore size below 3 nm. However, Fig. 3 and Table 1 indicate that the synthesized sol–gel AL-MCM-41 catalyst has pore size uniformity and considerable high pore volume and surface area. Pore volume was determined from the nitrogen adsorbed volume at $P/P^0 = 0.98$.

4.2. Catalytic activity of sol–gel and hydrothermal AL-MCM-41 for PP decomposition

Experiments were conducted for both catalytic and noncatalytic dynamic decomposition of PP in TGA (Fig. 4). The temperature at which maximum weight loss rate occurs (T_m) and the initial mass loss observed are reported in Table 2 for each case of the experiments. The initial mass loss observed was (2.55–12.11 wt%), which is due to presence of moisture in the catalyst. Reduction in T_m on application of catalysts (sol–gel Al-MCM-41) is shown through the sample derivative thermogravimetric (DTG) curves (Fig. 5). It is observed from the table and the figure that T_m reduces significantly, in comparison to noncatalytic decomposition, due to application of the catalyst. Table 2 reflects that thermal decomposition temperatures of PP are shifted to much lower temperatures in the presence of catalyst. The maximum reduction of T_m is observed to be 114 K for 32.5 wt% catalyst concentration. It is worth mentioning here that catalytic activity of mesoporous catalyst like Al-MCM-41 towards polymer decomposition mainly depends on the mesopore size that allows the movement of the polymer chain in the

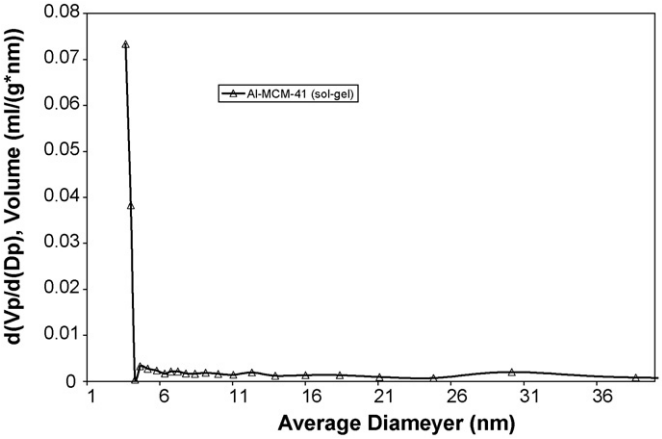

Fig. 3. BJH (adsorption) pore size distribution of Al-MCM-41 (sol–gel) catalyst.

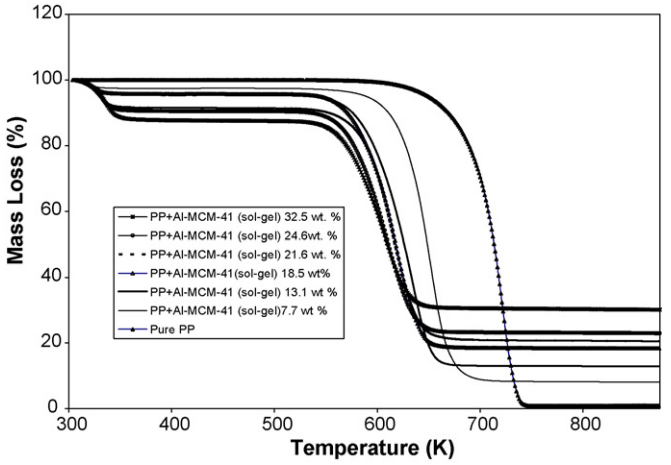

Fig. 4. Experimental TG curves for the catalytic pyrolysis of waste PP with different catalyst (Al-MCM-41 (sol–gel)) percentage.

pores, surface area that takes part in the decomposition reaction and the aluminium content (or number of acid sites) which is involved in such decomposition mechanism [7].

It is further observed from the figures (Figs. 4 and 5) that the shape of the curves changes significantly up to 13.1 wt% of the catalyst and afterwards the curves are overlapping in nature indicating less impact of the catalyst. Since, the catalyst is expensive and, at the moment, there are no useful ways to improve their short life or to make effective recycling [12], therefore, we concentrated on getting the optimum catalyst percentage. Economically optimum catalyst percentage should be decided based on the extent of decrease of decomposition temperature with catalyst percentage. Fig. 6 shows the gradually decreasing effect of catalyst percentage on ΔT_m (the change in T_m with respect to that for noncatalytic PP decomposition). It is further observed that the optimum catalyst percentage should be around 18.5 wt%, since, after that reduction in T_m with increase in catalyst percentage is not so significant. Hence, using catalyst percentage more than this would not be economically effective. Therefore, we selected 18.5 wt% as the optimum catalyst (sol–gel Al-MCM-41) percentage for the present study. The reduction in T_m is

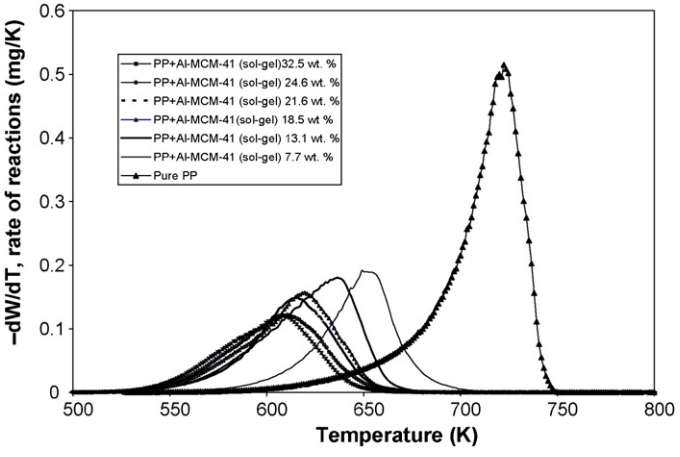

Fig. 5. Experimental DTG curves for the catalytic pyrolysis of waste PP with different catalyst (Al-MCM-41 (sol–gel)) percentage.

Table 2
Experimental conditions for TGA studies using Al-MCM-41 (sol–gel)

Catalyst	Catalyst percentage (%)	Total initial mass (mg)	Total initial mass loss (%)	T_m (K)
Al-MCM-41 (sol–gel)	7.7	9.53	2.55	652.53
	13.1	12.19	4.59	636.89
	16.4	19.09	2.79	625.81
	18.5	10.81	4.24	619.60
	21.6	10.70	8.41	616.69
	24.6	10.54	9.37	611.63
	32.5	12.11	12.11	608.98

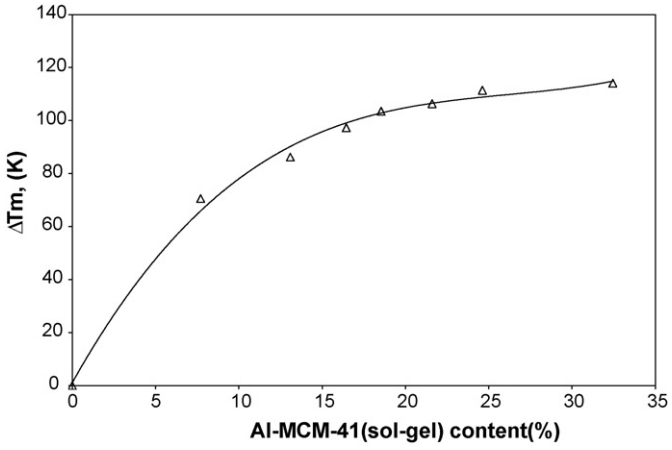

Fig. 6. Effect of catalyst concentration on reduction in maximum decomposition temperature.

around 103 °C at 18.5 wt%. It is also interesting to see from Fig. 4 that the TG curves with and without catalyst are constant pattern in nature. Only shift in the TG curves towards lower temperatures are observed due to application of catalyst and increase in catalyst percentage. This shift of the curves also slowly reduced at higher percentages of the catalyst indicating less effect of addition of further catalyst in the polymer sample. The constant pattern behaviour of the TG curves possibly suggests existence of similar reaction mechanism both under catalytic and noncatalytic decomposition of mesoporous Al-MCM-41. Here, large polymer fragments are cracked on the external surface of the catalyst and then enters into the mesopores where they get cracked further leading mainly to the higher olefins and liquid products [8,15]. This can only be confirmed after thorough analysis of the decomposition products. However, presence of catalyst surface cracks the polymer into comparatively smaller fractions and at least makes the decomposition of PP energy effective.

4.3. Decomposition kinetics analysis

In the present work, we have carried out nonisothermal decomposition of the PP sample at five different heating rates (5, 10, 15, 20, and 25 K min^{-1}) with the optimum catalyst percentage (18.5 wt%) and without catalyst. The temperature at which the conversion (α) is zero (T_{W_0}), decomposition starts (T_d), maximum weight loss rate occurs (T_m) and the end of pyrolysis step (T_{W_∞}) takes place have been reported in Table 3 for each case of the experiments. Table 3 reflects that thermal decomposition of PP starts at around 670 K and shows a maximum decomposition rate at 723 K at a heating rate of 10 K min^{-1}, which is shifted to much lower temperatures in the presence of catalyst. The shift is observed to be 103 K at a catalyst percentage of 18.5 wt%.

Figs. 7 and 8 represent the TG and DTG curves, respectively, for noncatalytic decomposition of PP at five different heating rates of 5, 10, 15, 20, and 25 K min^{-1}. Similarly, Figs. 9 and 10 represent the TG and DTG curves, respectively, for catalytic (sol–gel Al-MCM-41) decomposition of PP at five different heating rates of 5, 10, 15, 20, and 25 K min^{-1} at a catalyst percentage of 18.5 wt%. It is observed from the figures (Figs. 7 and 9) that the TG curves show constant pattern behaviour and higher heating rate finishes the decomposition phenomenon faster. The constant pattern behaviour is attributed to the fact of similar reaction mechanism (as discussed earlier), which is the basis of multi-heating rate approach for kinetics analysis [3,5,16–27]. This is also supported by the almost simi-

Table 3
Experimental conditions for catalytic (Al-MCM-41 (sol–gel)) and noncatalytic TGA studies

Sample	Initial mass (mg)	Heating rate (K min^{-1})	Temperature range (K)	$T_{W_0}/T_d/T_m/T_{W_\infty}$ (K)
PP	19.77	5	303–875	533.6/596.9/706.8/773.9
	20.32	10	303–875	526.9/670.0/723.07/749.8
	20.67	15	303–875	527.8/684.6/731.4/777.6
	19.78	20	303–875	527.5/684.8/736.8/770.2
	19.41	25	303–875	527.1/696.6/742.9/785.7
PP+Al-MCM-41 (18.5 wt%)	7.48	5	303–873	489.3/535.1/608.6/669.9
	10.35	10	303–873	473.2/576.6/619.6/682.3
	13.59	15	303–873	461.7/596.3/637.6/700.9
	10.80	20	303–873	464.4/605.2/640.7/717.5
	9.09	25	303–873	461.9/607.9/649.0/711.0

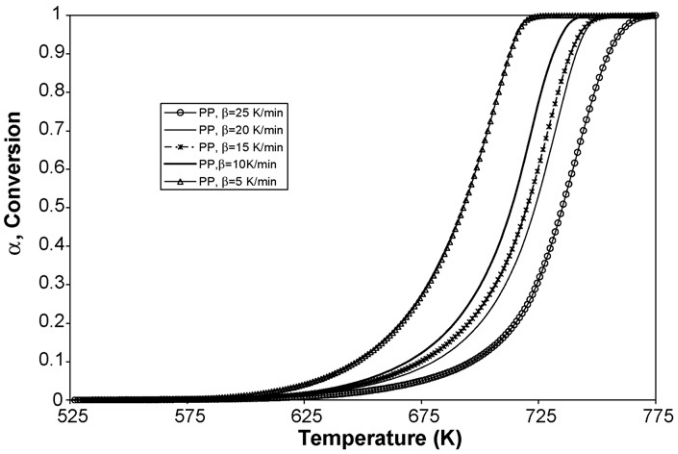

Fig. 7. Variation of conversion (α) with temperature during noncatalytic nonisothermal pyrolysis of PP sample.

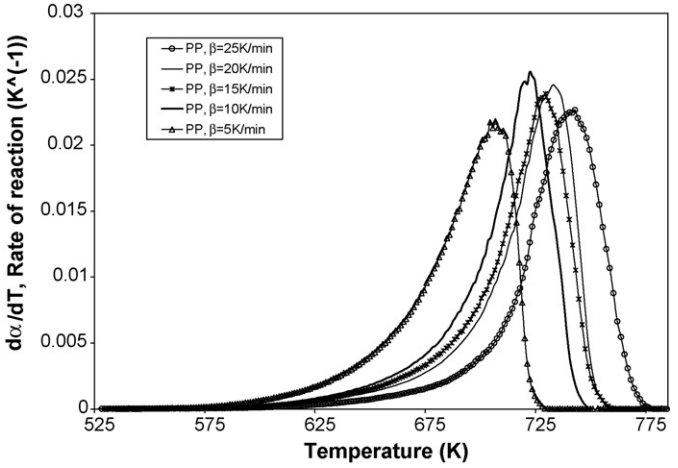

Fig. 8. Variation of rate of decomposition (dα/dT) with temperature during noncatalytic nonisothermal pyrolysis of PP sample.

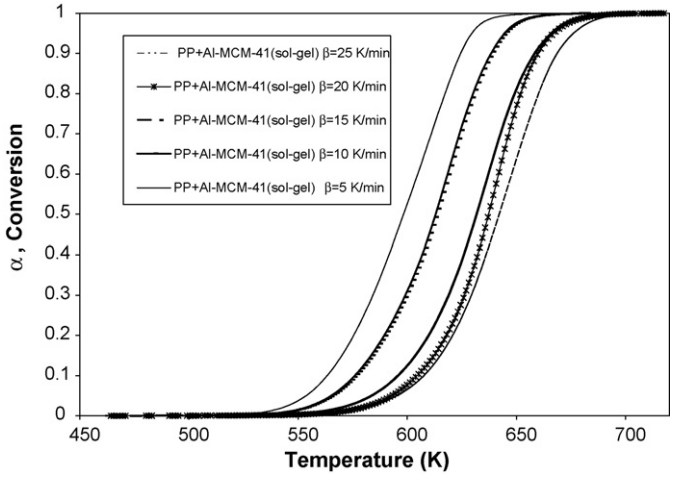

Fig. 9. Variation of conversion (α) with temperature during catalytic nonisothermal pyrolysis (18.5 wt% catalyst) of PP sample.

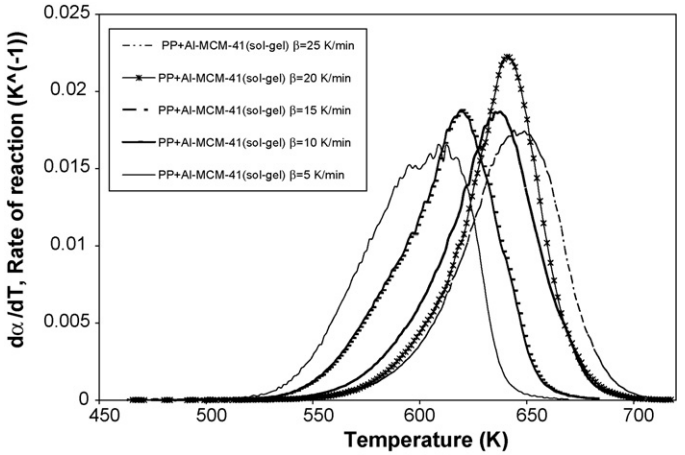

Fig. 10. Variation of rate of decomposition (dα/dT) with temperature during catalytic nonisothermal pyrolysis (18.5 wt% catalyst) of PP sample.

lar peak height and constant pattern behaviour of the DTG curves (Figs. 8 and 10) both for the noncatalytic and catalytic decomposition of PP. We can also clearly notice the single peak in the DTG curves both for the catalytic and noncatalytic decomposition of PP.

4.4. Kinetics for nonisothermal model-free analysis

Dependency of E_α on α obtained for nonisothermal decomposition of the PP sample with and without catalyst is presented through Fig. 11. With the repeatability data during thermal analysis of PP, we performed the error analysis in terms of percentage average relative deviation (ARD%) in E_α for three different sets of data using the relation, $\mathrm{ARD}\,(\%) = (100/N)\sum_{i=1}^{N}|(x_i^{\mathrm{cal}} - x_{\mathrm{av},i}^{\mathrm{cal}})/x_{\mathrm{av},i}^{\mathrm{cal}}|$. Here, x_i^{cal} and $x_{\mathrm{av},i}^{\mathrm{cal}}$ are the calculated values of E_α for a particular set and average value of E_α including all the three sets. N is the total number of data points for each set. The resulting ARD% is 1.170161, 1.25178, and 0.238782% for the three sets. It is observed from the figure (Fig. 11) that for both

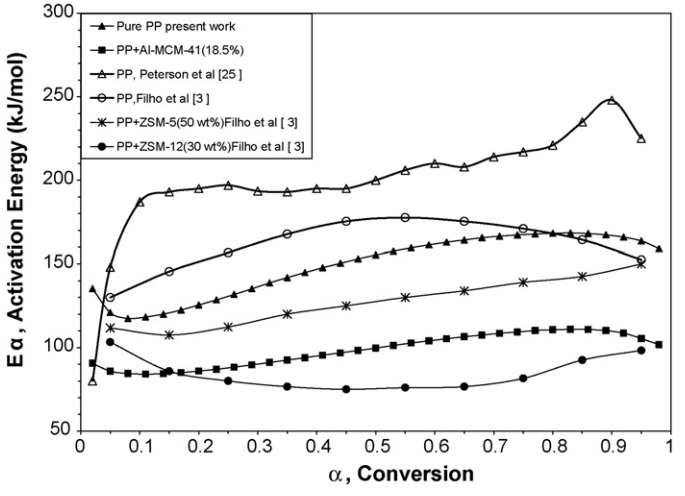

Fig. 11. Dependency of activation energy on conversion of catalytic and noncatalytic nonisothermal decomposition of PP sample (present work and literature reported data).

catalytic and noncatalytic decomposition, E_α is a slowly increasing function of α in the range ($0.1 \leq \alpha \leq 0.9$). E_α for catalytic decomposition is much lower than that for noncatalytic one. It is also observed that the difference in E_α between noncatalytic and catalytic decomposition is also slowly increasing with α. However, exactly similar trends for catalytic and noncatalytic cases for any value of α further justifies the fact that similar reaction mechanism might be followed for both the cases of decomposition leading mainly to the higher olefins and liquid products [8,15]. Thus, only effect of catalyst is observed in the form of reduction of the temperature and the activation energy. Studies of Peterson et al. [25] and Filho et al. [3] on variation of E_α with α for noncatalytic decomposition of pure PP are compared with the present result in the same figure. It is observed that the trends of variation reported by them are similar to that observed by us. In the present investigation, we used PP sample of melt flow index (MFI) 3.0, whereas Filho et al. [3] used PP sample of higher melt flow index 11.5, i.e. of lower molecular weight but with filler calcium carbonate (12 wt%). Peterson et al. [25] used PP sample of average molecular weight (12,000). Therefore, the existing differences in the activation energy might be due to different molecular weights of the PP samples used for the different cases as well as due to the effect of the inorganic filler in the PP sample used by Filho et al. [3]. Zeolite molecular sieve (ZSM) catalyzed results of Filho et al. [3] on PP are also compared with the present result in the same figure. It can be observed that our catalyst is superior to the ZSM-5 catalyst used by Filho et al. [3] in terms of catalyst loading. Similar type of reduction of activation energy is obtained in the present case with much less catalyst (18.5 wt%) in comparison to ZSM-5 catalyst (50.0 wt%) used by Filho et al. [3]. Though ZSM-12 is found to be better performing than our catalyst, the catalyst percentage (18.5 wt%) used in the present case is much lower than that used by Filho et al. [3] (30 wt%). The strong and increasing values of E_α with α at the later part of ZSM-5 catalyzed decomposition (Fig. 11) is just opposite to the trend observed in case of Al-MCM-41 catalyzed decomposition. This may be explained as follows. Large polymer fragments are cracked on the external surface of the catalysts at the start of decomposition and then enter into the available mesopores where they get cracked further leading mainly to the higher olefins and liquid products. This is possibly a common phenomenon both for mesoporous and microporous catalysts. Thus, only effect of catalyst is observed in the form of reduction of the temperature and the activation energy at this stage of decomposition. At the later stage of ZSM-catalyzed decomposition, the reaction mechanism possibly takes different path for oligomerization, cyclization, and hydrogen transfer reactions particularly in the micropores leading to higher activation energy [3]. The diffusional resistances become predominant for catalysts with comparable pore sizes, i.e. the micropores. Therefore, it is expected that catalyst with wide pore size would give less diffusional resistance and would be more effective towards decomposition of PP. Further, according to Filho et al. [3] the used ZSM-12 catalyst, formed by a 12 ring member with 5.6 Å × 6.0 Å, had smaller crystallite size and greater external macropore and mesopore surface in comparison to the ZSM-5 used, formed by a 10 ring member with 5.3 Å × 5.6 Å. Therefore, the ZSM-12 catalyst have been more efficient in the degradation activity for PP in comparison to ZSM-5. Similarly, the Al-MCM-41 catalyst in the present case, due to existence of larger external macropore and mesopore surface in it, also show better catalytic activity in comparison to ZSM-5 for decomposition of PP. The similar trend of both ZSM-5 and ZSM-12 catalysts at the later stage of conversion (Fig. 11) might be due to their microporous activity, which is not the case for the mesoporous Al-MCM-41 catalyst.

5. Conclusion

Both thermal and catalytic decomposition of PP sample is studied to understand the effect of catalyst Al-MCM-41, synthesized by sol–gel method, on the decomposition behaviour. Results show that catalytic decomposition starts and completes at much lower temperatures than that for noncatalytic decomposition. It is observed that the temperature decreases exponentially with catalyst percentage. It is further observed that the optimum catalyst percentage was around 18.5 wt%, where the reduction in maximum decomposition temperature is around 103 °C. The nonlinear Vyazovkin model-free technique is applied to evaluate the quantitative information on variation of E_α with α for the PP sample under both catalytic and noncatalytic nonisothermal conditions. The constant pattern behaviour of the TG curves and the similar trend on variation of E_α with α for both catalytic and noncatalytic decomposition of PP indicates similar mechanism involved during decomposition. From the comparison of the effects of other catalysts on PP samples, it is found that our catalyst is superior to the ZSM-5 catalyst used by Filho et al. [3] in terms of catalyst loading but ZSM-12 with higher percentage (30 wt%) is found to be better performing than our catalyst (18.5 wt%). Better catalytic activity observed for ZSM-12 as reported by Filho et al. [3] and Al-MCM-41 in the present case is possibly due to existence of less diffusional resistances because of larger pores in the catalysts. The opposite behaviour on variation of E_α with α at the later part of ZSM-5 and ZSM-12 catalyzed decomposition is possibly due to reaction mechanisms like oligomerization, cyclization, and hydrogen transfer reactions taking place inside the micropores pores of the ZSM catalysts.

References

[1] G. Karishma, G. Manos, Polym. Degrad. Stab. 86 (2004) 225.
[2] A. Marcilla, A. Gómez, J.A. Reyes-Labarta, A. Giner, F. Hernández, J. Anal. Appl. Pyrol. 68–69 (2003) 467.
[3] J.G.A.P. Filho, E.C. Graciliano, A.O.S. Silva, M.J.B. Souza, A.S. Araujo, Catal. Today 107–108 (2005) 507.
[4] Q. Zhou, L. Zheng, Y.Z. Wang, G.M. Zhao, B. Wang, Polym. Degrad. Stab. 84 (2004) 493.
[5] A. Durmus, S.N. Koc, G.S. Pozan, A. Kasgoz, Appl. Catal. B 61 (2005) 316.
[6] C. Vasile, H. Pakdel, B. Mihai, P. Onu, H. Darie, S. Ciocâlteu, J. Anal. Appl. Pyrol. 57 (2001) 287.
[7] A. Marcilla, A. Gómez-Siurana, D. Berenguer, Appl. Catal. A 301 (2006) 222.
[8] Y.H. Lin, H.Y. Yen, Polym. Degrad. Stab. 89 (2005) 101.
[9] P. Onu, C. Vasile, S. Ciocilter, E. Iojoiu, H. Darie, J. Anal. Appl. Pyrol. 49 (1999) 145.

[10] Y.H. Lin, M.H. Yang, Appl. Catal. B 69 (2006) 145.
[11] J. Aguado, D.P. Serrano, J.M. Escola, E. Garagorri, J.A. Fernández, Polym. Degrad. Stab. 69 (2000) 11.
[12] A. Marcilla, A. Gómez, J.A. Reyes-Labarta, A. Giner, F. Hernández, Polym. Degrad. Stab. 80 (2003) 233.
[13] R.A. García, D.P. Serrano, D. Otero, J. Anal. Appl. Pyrol. 74 (2005) 379.
[14] J. Aguado, D.P. Serrano, G. San Miguel, J.M. Escola, J.M. Rodríguez, J. Anal. Appl. Pyrol. 78 (2007) 153.
[15] D.P. Serrano, J. Aguado, J.M. Escola, J.M. Rodríguez, G. San Miguel, J. Anal. Appl. Pyrol. 74 (2005) 370.
[16] B. Saha, A.K. Maiti, A.K. Ghoshal, Thermochim. Acta 444 (2006) 46.
[17] P. Carniti, A. Gervasini, Thermochim. Acta 379 (2001) 51.
[18] S. Vyazovkin, V. Goriyachko, Thermochim. Acta 194 (1992) 221.
[19] S. Vyazovkin, C.A. Wight, Thermochim. Acta 340–341 (1999) 53.
[20] S. Vyazovkin, Thermochim. Acta 355 (2000) 155.
[21] S. Vyazovkin, C.A. Wight, Chem. Mater. 11 (1999) 3386.
[22] S. Vyazovkin, D. Dollimore, J. Chem. Inf. Comput. Sci. 36 (1996) 42.
[23] S. Vyazovkin, Int. J. Chem. Kinet. 28 (1996) 95.
[24] S. Vyazovkin, N. Sbirrazzuoli, Macromol. Rapid Commun. 27 (2006) 1515.
[25] J.D. Peterson, S. Vyazovkin, C.A. Wight, Macromol. Chem. Phys. 202 (2001) 775.
[26] B. Saha, A.K. Ghoshal, Thermochim. Acta 451 (2006) 27.
[27] B. Saha, A.K. Ghoshal, Thermochim. Acta 453 (2006) 120.
[28] A. Matsumoto, H. Chen, K. Tsutsumi, M. Grün, K. Unger, Microporous Mesoporous Mater. 32 (1999) 55.
[29] M.M.L. Ribeiro Carrott, F.L. Conceição, J.M. Lopes, P.J.M. Carrott, C. Bernardes, J. Rocha, F. Ramôa Ribeiro, Microporous Mesoporous Mater. 92 (2006) 270.